

Inverse filtering procedure to correct cone penetration data for thin-layer and transition effects

R.W. Boulanger & J.T. DeJong

Department of Civil and Environmental Engineering, University of California, Davis, USA

ABSTRACT: This paper presents an inverse filtering procedure for developing estimates of “true” cone penetration tip resistance and sleeve friction values from measured cone penetration test data in interlayered soil profiles. Results of prior studies of cone penetration in layered soil profiles are utilized for developing and evaluating the inverse filtering procedure. The inverse filtering procedure has three primary components: (1) a model for how the cone penetrometer acts as a low-pass spatial filter in sampling the true distribution of soil resistance versus depth, (2) a solution procedure for iteratively determining an estimate of the true cone penetration resistance profile from the measured profile given the cone penetration filter model, and (3) a procedure for identifying sharp transition interfaces and correcting the data at those interfaces. The details of the inverse filtering procedure presented herein were developed with a focus on liquefaction problems, but the concepts and framework should be applicable to other problems. Example applications of the inverse filtering procedure are presented for four CPT soundings illustrative of a range of soil profile characteristics. The proposed procedure provides an objective, repeatable, and automatable means for correcting cone penetration test data for thin-layer and transition zone effects.

1 INTRODUCTION

The cone penetration test (CPT) provides excellent stratigraphic detail and information for estimating a wide range of soil properties, but the spatial resolution of cone tip resistance (q_t) and sleeve friction (f_s) measurements is still limited by the physical volume of soil around a cone tip that influences those measurements. Measurements of q_t are most strongly influenced by soils within about 10–30 cone diameters (d_c) of the cone tip, which corresponds to influence zones of 0.35–1.3 m thickness for standard 10 cm² and 15 cm² cones. Measurements of q_t and f_s therefore depend on the sequence and properties of all soils within the zone of influence, such that the cone acts as a low-pass spatial filter on the true distribution of soil resistance in a soil profile. This physical low-pass spatial filtering removes information at the shorter physical wavelengths [m], corresponding to higher spatial frequencies [cycles/m], that are necessary for defining sharp interfaces between soils with different properties. The resulting spatial smoothing of information at interfaces in interbedded soil deposits is well recognized in practice (e.g., Lunne et al. 1997, Mayne 2007) and has been the focus of considerable study.

The loss of detail at shorter physical wavelengths during cone penetration in layered soil profiles may not be of importance in some areas of practice,

but there are certain situations where the resulting “thin layer” and “transition zone” effects can be sufficiently important to warrant evaluating. For example, thin layer effects can be important for liquefaction methodologies, depending on the analysis procedures, soil conditions, and seismic loading (as discussed in Boulanger et al. 2016). The use of simplified one-dimensional (1D) liquefaction vulnerability indices (LVIs) can overestimate the potential for liquefaction induced deformations if the predicted intervals of liquefaction triggering are primarily associated with numerous thin layers or transition zones. In other cases, the results of 1D-LVI’s may be insensitive to thin layer and transition zones if those zones are a small portion of the predicted intervals of liquefaction triggering. For nonlinear dynamic analyses (NDAs) of sites with interbedded soils, the representative properties assigned to the liquefiable interlayers can similarly benefit from accounting for thin layer and transition zone effects in some situations and be relatively unaffected in others. More commonly, thin layer and transition zone effects are just one factor among several that can contribute to an accumulation of conservatism or bias in predicted behaviors (e.g., Boulanger et al. 2016, Munter et al. 2017, Cox et al. 2017).

This paper presents an inverse filtering procedure for developing estimates of “true” cone penetration tip resistance and sleeve friction values

from measured cone penetration test data. Results of prior studies are briefly reviewed and the available theoretical and experimental data for thin layer and transition zone effects in idealized two—and three-layer soil profiles are utilized for developing the inverse filtering procedure. The inverse filtering procedure and each of its three primary components are described, including: (1) the model for how the cone penetrometer acts as a low-pass spatial filter in sampling the true distribution of soil resistance versus depth, (2) the solution procedure for iteratively determining an estimate of the true cone penetration resistance profile from the measured profile given the cone penetration filter model, and (3) the procedure for identifying sharp transition interfaces and correcting data at those interfaces. Example applications of the inverse filtering procedure are then presented for four CPT soundings illustrative of a range of soil profile characteristics. The proposed procedure, which is easy to automate and perform, is shown to work well for a range of stratigraphies. It is hoped that future experience with application of the procedure in practice will lead to further improvements.

2 PAST STUDIES OF PENETRATION IN LAYERED SOIL PROFILES

Thin layer and transition zone effects have been studied extensively, including contributions from the authors listed in Table 1. These studies have

utilized elastic analyses, nonlinear analyses (cavity expansion and axisymmetric models), and physical measurements (1 g physical models, centrifuge models, field data). In all cases except the elastic analyses by Yue and Yin (1999), these studies have focused on idealized profiles with two or three uniform soil layers in different sequences; e.g., a stronger soil over a weaker soil, a weaker soil over a stronger soil, a stronger soil layer embedded in weaker soil, or a weaker soil layer embedded in a stronger soil.

The schematic in Figure 1 shows the case of a sand layer embedded in a clay deposit to illustrate both the thin layer and transition zone effects. The measured tip resistance (denoted as q^m) will smoothly increase as the cone approaches and enters the stronger layer and then smoothly decrease as the cone approaches and then enters the underlying weaker soil. The “true” tip resistance (denoted as q^t) is the value that would have been measured in this same soil if the measurement was free of the influence of the overlying and underlying weaker clay soils. The “transition” zones are those intervals near the layer interfaces over which q^m smoothly increases or decreases even though q^t abruptly changes. The thin layer effect occurs when the peak q^m becomes smaller than the corresponding q^t , with the error increasing as the stronger layer’s thickness decreases. The thin layer factor (K_H), defined as q^t divided by the peak q^m for the layer, therefore increases as layer thickness decreases.

Table 1. Past studies of cone penetration in layered soil profiles.

Authors	Primary focus
<i>Elastic analyses:</i>	
Sayed & Hamed (1987)	Spherical and cylindrical cavity expansion in layered elastic system
Vreugdenhil et al. (1994)	Elastic solutions for stress distributions in layered elastic system
Yue & Yin (1999)	Elastic solutions for stresses in a multi-layered system
<i>Nonlinear analyses:</i>	
Van den Berg et al. (1996)	Axisymmetric penetration analysis in layered sand and clay
Ahmadi & Robertson (2005)	Axisymmetric penetration analysis in layered sand and clay
Xu & Lehane (2008)	Spherical cavity expansion analogue for layered sand and clay
Walker & Yu (2010)	Axisymmetric penetration analysis in layered clay
Mo et al. (2017)	Cavity expansion analysis for layered sand and clay.
<i>Physical data:</i>	
Treadwell (1976)	Chamber tests of cone penetration in layered sand
Meyerhof & Valsangka (1977)	Model tests of piles and cones in layered sand and clay
Foray & Pautre (1988)	Chamber tests of cone penetration in layered sand
Canou (1989)	Chamber tests of cone penetration in layered sand
Youd et al. (2001)	Interpretation of field data
Hird et al. (2003)	Chamber tests of piezocones for thin sand/silt layers in clay
Silva & Bolton (2004)	Centrifuge tests of cone penetration in layered sand
Mlynarek et al. (2012)	Chamber tests of cone penetration in layered sand and clay
Mo et al. (2015)	Centrifuge tests of cone penetration in layered sand
Tehrani et al. (2018)	Chamber tests of cone penetration in layered sand

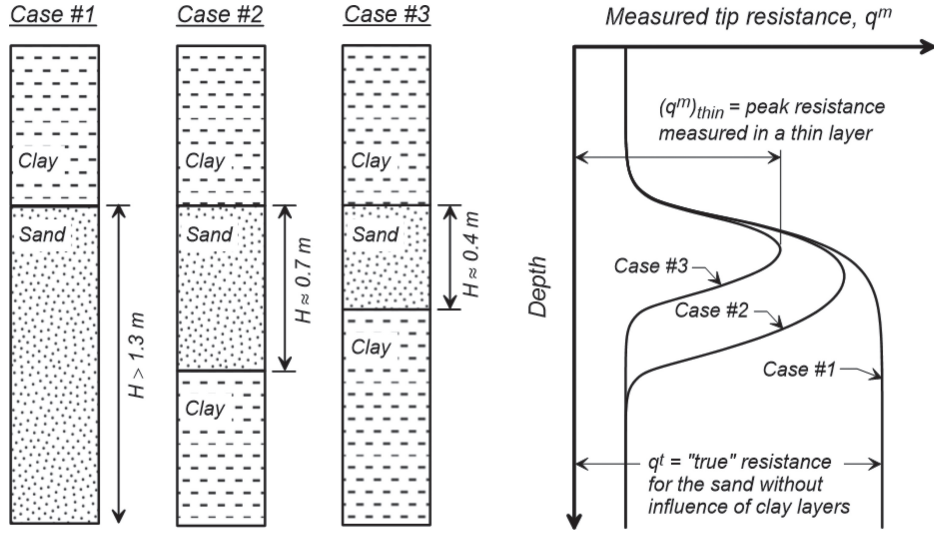


Figure 1. Schematic of thin layer effect for a sand layer embedded in a clay layer (modified from Robertson and Fear 1995).

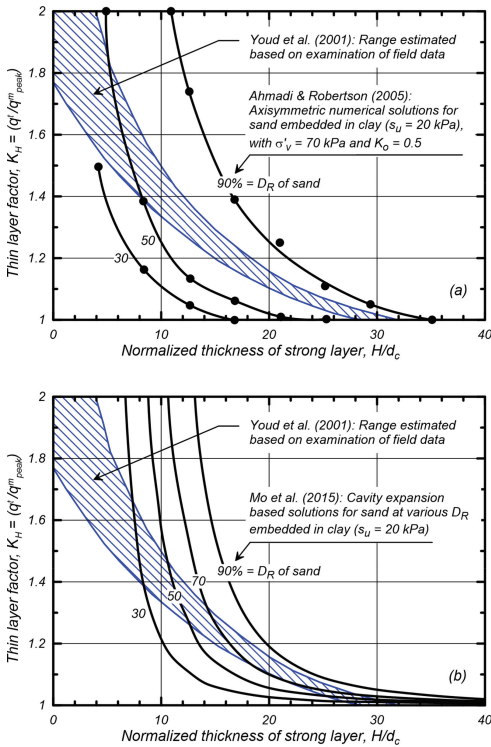


Figure 2. Thin layer factors inferred from field data (Youd et al. 2001) compared to: (a) axisymmetric numerical analyses by Ahmadi and Robertson (2005), and (b) cavity expansion based solutions by Mo et al. (2017).

Thin layer factors from three different studies are plotted versus normalized layer thickness (H/d_c) in Figures 2a and 2b to illustrate the range of findings in the literature. The range presented by Youd et al. (2001), and shown in both figures for reference purposes, was inferred from examinations of field data, although the details of the field data and interpretation method were not described. The results shown for Ahmadi and Robertson (2005) in Figure 2a are from axisymmetric nonlinear analyses of a sand layer with relative densities (D_R) of 30, 50 and 90% with $\sigma'_v = 70$ kPa and $K_o = 0.5$ (producing q^t of about 3.2, 5.8, and 22 MPa, respectively) embedded in soft clay with an undrained shear strength (s_u) of 20 kPa (producing a q^t of about 0.9 MPa). The corresponding thin layer factors increased with the D_R of the sand layer, which alternatively can be identified as having $q^t_{\text{strong}}/q^t_{\text{weak}}$ ratios of about 3.6, 6.4, and 24, respectively. Ahmadi and Robertson (2005) also showed their thin layer factors to decrease with increasing effective confining stress, which is consistent with the dependence of sand dilation angle on confining stress used in their analyses. The results shown for Mo et al. (2017) in Figure 2b are based on cavity expansion analyses for a sand layer with D_R of 30, 50, 70, and 90% embedded in clay ($s_u = 20$ kPa), with the properties chosen to be equivalent to those used by Ahmadi and Robertson (2005). The corresponding thin layer factors are similar to those of Ahmadi and Robertson (2005), but become steeper and exceed values of 2.0 at larger values

of the normalized layer thickness. The $q_{\text{strong}}^t/q_{\text{weak}}^t$ ratios for the cases analyzed by Mo et al. (2017) were not reported, but should be similar to those for the cases analyzed by Ahmadi and Robertson (2005). The results of these and other studies for idealized three-layer profiles produce K_H values that are less than about 1.1 when the strong layer thickness is greater than about 30 cone diameters, increase as the $q_{\text{strong}}^t/q_{\text{weak}}^t$ ratio increases, and can exceed values of 2.0 for layers that are less than about 10 cone diameters thick if the $q_{\text{strong}}^t/q_{\text{weak}}^t$ ratio is large enough.

Transition zones in idealized two layer profiles can also be described in terms of the sensing and development distances. When the cone tip is in the upper layer, the sensing distance is defined as the greatest distance between the cone tip and the top of the underlying layer for which q^m in the upper layer is “affected” by the underlying layer. When the cone tip is in the lower layer, the development distance is defined as the greatest distance between the top of the underlying layer and the cone tip for which q^m in the underlying layer is still “affected” by the upper layer. Specific criteria for determining sensing and development distances are often not reported, but appear to represent some degree of visually apparent effects (e.g., perhaps a few percent). Sensing and development distances and the equations describing how q^m varies from q_{strong}^t to q_{weak}^t and from q_{weak}^t to q_{strong}^t are often assumed to be mirror images of each other (e.g., Xu and Lehane 2008, Mo et al. 2015), which is an approximation that implies equal influence of the soil resistance in front of and behind the cone tip. In reality, experimental and theoretical studies (e.g., Ahmadi and Robertson 2005, Tehrani et al. 2018) show that sensing distance in a strong layer over a weak layer is greater than the development distance in a strong layer under a weak layer, which indicates that soils in front of the cone tip have a greater influence on penetration resistance than the soils behind the cone tip. Sensing and development distances in a strong layer adjacent to a weak layer increase as the ratio of the soil layer strengths increases (e.g., Xu and Lehane 2008). Sensing and development distances in a weak soil adjacent to a stronger soil are smaller than those for the stronger soil, and they decrease as the ratio of the soil layer strengths increases. For example, Walker and Yu (2010) show that q^t for a soft clay layer embedded in stronger clay can be almost fully developed in layers as thin as 2–3 cone diameters.

Application of thin-layer or transition zone corrections in practice is relatively uncommon due to a number of challenges. Their application to field situations is generally subjective, such that the corrections applied can vary significantly between different individuals analyzing the same data. The

ability to consistently distinguish between sharp interfaces and graded interfaces (e.g., upward or downward fining sequences) is uncertain. The procedures are difficult to automate, and time consuming to apply in the absence of an automated processing method. These challenges, combined with the fact that the results may only have a modest effect for many design/evaluation problems, appears to be why their use is relatively uncommon.

3 INVERSE FILTERING PROCEDURE

Inverse filtering is widely used in image and signal processing for a wide range of measurement applications (e.g., Cristobal et al. 2011). Inverse filtering can help restore or improve the quality of an image or measurement if a good model can be developed for the function that “blurred” the measurement and if the signal-to-noise ratio in the measurement is favorable. Inverse filtering often responds poorly to any noise present in the measurement because noise tends to be at high spatial frequencies and the blurred measurement tends to be weakest (i.e., have the lowest signal strength) at high spatial frequencies.

The application of inverse filtering techniques to cone penetration data begins with the assumption that there is a “true” cone penetration resistance that would be obtained if the cone penetration test data were dependent solely on the soil properties at a point (i.e., measured by an infinitely small cone without particle size effects). The measured cone penetration resistance depends on soil properties within a zone of influence around the cone tip, such that cone penetration acts as a low-pass spatial filter in sampling the true profile; i.e., strong variations in soil properties over short distances correspond to short wavelengths (or high spatial frequencies) that are masked or filtered by the cone penetration process. An inverted cone penetration resistance is obtained by applying an inverse cone penetration filter to the measured cone penetration resistance profile.

It is convenient to simplify notation for cone penetration resistances for the present purposes as follows. True, measured, and inverted cone penetration resistances are identified with superscripts as q^t , q^m , and q^{inv} , respectively. The q^m refers to the resistance after any correction for unequal area effects (i.e., pore pressure behind the cone tip) has already been applied, and all three terms are normalized by atmospheric pressure. The conventional subscripts for identifying cone penetration resistances as corrected for unequal area effects or normalized by atmospheric pressure (e.g., q_{1N}) are omitted for clarity.

The filtering effect of the cone penetration process can now be expressed as,

$$q^m(z) = q'(z) * w_c(z) \quad (1)$$

where the asterisk indicates convolution of q' with the cone penetration filter (w_c). Convolution refers to the integral of the point-wise multiplication of the two functions as a function of the amount that one of the functions is shifted relative to the other. The spatial filtering effect can alternatively be expressed as,

$$q^m(z) = \int_{z_{\min}}^{z_{\max}} q'(\tau) w_c(z - \tau) d\tau \quad (2)$$

The convolution integration limits, which are $-\infty$ to ∞ for the general case, are set equal to the depth limits for the CPT sounding (i.e., z_{\min} to z_{\max}), which also ensures that the q^m vector retains the same length as the q' vector.

The inversion of this filtering process is complicated by the strongly nonlinear nature of w_c and limitations on the highest spatial frequencies (shortest physical wavelengths) for which the inversion is meaningful. For cone penetration, the highest spatial frequencies for which the measurements may contain meaningful information could be governed by either the data sampling interval or the physical size of the cone. Higher spatial frequencies than are measurable can exist in the field, such as those associated with discrete jumps in q' across interfaces, but these higher spatial frequencies almost certainly cannot be reliably inverted from the measurements. For this reason, the inverse filtering procedure must include steps that remove any of these higher spatial frequency components from the solution, as discussed later.

The inverse filtering procedure proposed herein has three primary components: (1) a model for how the cone penetrometer acts as a low-pass spatial filter in sampling the true distribution of soil properties versus depth, (2) a solution procedure for iteratively determining an estimate of the true cone penetration resistance profile from the measured profile and cone penetration filter model, and (3) a procedure for identifying sharp transition interfaces and correcting the data at those interfaces. The following sections address each of these three components.

4 CONE PENETRATION FILTER MODEL

Any cone penetration filter model needs to account for the primary influencing factors, recognizing that a perfect filter model with the full complexity

of factors is not yet realizable. The proposed filter model for the current study is expressed as a function of the q' profile alone, though additional information from f_s , u_{bt} , V_s , or other measurements may prove beneficial. The function forms and parameters for the current model were developed to be consistent with the body of results from prior studies regarding thin layer effects and sensing/development distances (Table 1), including their dependencies on various soil profile characteristics as discussed in the previous section.

The cone penetration filter (w_c) model, shown in Figure 3, is the normalized product of two functions, w_1 and w_2 , as,

$$w_c = \frac{w_1 w_2}{\sum w_1 w_2} \quad (3)$$

where w_c , w_1 , and w_2 are all functions of z' , which is the depth relative to the cone tip normalized by the cone diameter (d_c),

$$z' = \frac{z - z_{tip}}{d_c} \quad (4)$$

where z_{tip} is the current depth of the cone tip. The dependence of w_c , w_1 , and w_2 on z' is omitted from notation for simplicity.

The w_1 term accounts for the relative influence of any soil decreasing with increasing distance from the cone tip as,

$$w_1 = \frac{C_1}{1 + \left(\frac{z'}{z'_{50}}\right)^{m_z}} \quad (5)$$

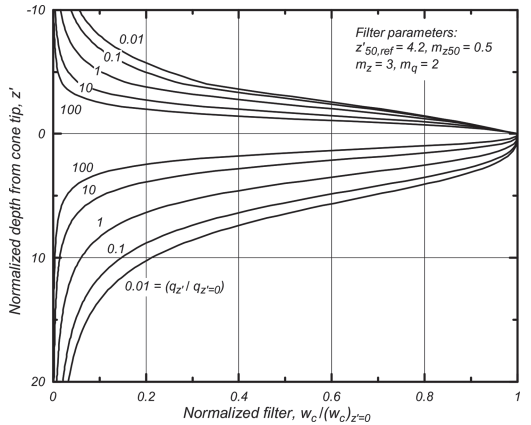


Figure 3. Normalized cone penetration filter versus normalized depth from the cone tip with lines for $q'_z / q'_{z=0} = 0.01, 0.1, 1, 10,$ and 100 .

where z'_{50} is the normalized depth at which $w_1 = 0.5C_1$, and the exponent m_z is a parameter that adjusts the variation of w_1 with z' . The parameter C_1 is equal to unity for points below the cone tip, and linearly reduces to a value of 0.5 for points located more than 4 cone diameters above the cone tip as,

$$\begin{aligned} C_1 &= 1 \quad \text{for } z' \geq 0 \\ &= 1 + \frac{z'}{8} \quad \text{for } -4 \leq z' < 0 \\ &= 0.5 \quad \text{for } z' < -4 \end{aligned} \quad (6)$$

The value of z'_{50} is computed as,

$$z'_{50} = 1 + 2 \left(C_2 z'_{50,ref} - 1 \right) \left(1 - \frac{1}{1 + \left(\frac{q'_{z'=0}}{q'_{z'}} \right)^{m_{50}}} \right) \quad (7)$$

where the product $C_2 z'_{50,ref}$ corresponds to the value of z'_{50} whenever $q'_{z'}$ is equal to q' at the cone tip (i.e., $q'_{z'=0}$). The parameter C_2 is equal to unity for points below the cone tip, and less than unity (0.8 is used herein) for points above the cone tip. Thus, $z'_{50,ref}$ is the value of z'_{50} for points below the cone tip whenever $q'_{z'}$ is equal to q' at the cone tip.

The w_2 term adjusts the relative influence that soils away from the cone tip will have on the penetration resistance based on whether those soils are stronger or weaker than the soil immediately at the cone tip. If the soil at a given depth is weaker than the soil at the cone tip, its relative influence on the penetration resistance is increased, and vice versa if it is stronger than the soil at the cone tip. The w_2 term is computed as,

$$w_2 = \frac{2}{\sqrt{1 + \left(\frac{q'_{z'}}{q'_{z'=0}} \right)^{m_q}}} \quad (8)$$

where the exponent m_q is a parameter that adjusts the variation of w_2 with $q'_{z'}/q'_{z'=0}$.

The resulting filter model is shown in Figure 3 as w_c (normalized by w_c at the cone tip) versus z' for $q'_{z'}/q'_{z'=0}$ values of 0.01, 0.1, 1, 10, and 100 for the baseline set of parameters: $z'_{50,ref} = 4.0$, $m_z = 3.0$, $m_{50} = 0.5$, and $m_q = 2$. The soils above the cone tip receive about one half the weight received by the soils below the cone tip, all else being equal (i.e., comparing the relative areas under the w_c curves). For this parameter set, the filter model predicts that the measured penetration resistance will be controlled by soils within 2–3 diameters of the cone tip if they are far weaker than the soils fur-

ther away (e.g., $q'_{z'}/q'_{z'=0} = 100$ at larger distances). Conversely, the measured penetration resistance will be significantly affected by soils as far as 15–20 diameters below the cone tip if the soils at these larger distances are far weaker than the soils near the cone tip (e.g., $q'_{z'}/q'_{z'=0} = 0.01$ at the larger distances). For more uniform soil profiles with only modest variations in q' , the measured penetration resistance is controlled by soils within about 9 cone diameters of the tip. In addition, the asymmetry of the filter model is required to simulate the observed asymmetry in the sensing and development distances for strong layers embedded in weaker soil.

The filter convolution process is illustrated for a two-layer profile in Figure 4. For this illustration, the cone tip has reached the middle of a stronger layer embedded in a weaker soil profile, as depicted by the profile of q' . The variation of w_c with depth is shown for that present cone tip depth. The q' vector is point-wise multiplied by the w_c vector and the product summed to obtain the value of q^m for the present cone tip depth, which is shown as the single solid symbol on the right hand plot. This process is repeated for all other cone tip depths (with w_c shifting accordingly) to arrive at the profile of q^m shown as a dashed line on the right hand plot. For the cone tip at the middle of the stronger layer, the filter w_c decreases with distance from the cone tip in either direction for points in the stronger layer (since $q'_{z'}/q'_{z'=0} = 1$ throughout the layer), but steps up to larger values at the interface with the weaker soil because $q'_{z'}/q'_{z'=0} \ll 1$ for points in the weaker soil (which increases w_c as shown in Figure 3).

The numerical evaluation of the convolution integral involved two other details. First, the filter window was truncated at a length of 60 cone diameters, centered at the cone tip (i.e., $-30 \leq z' \leq 30$), for the examples presented in this paper. This truncation reduces computations and has minimal effect on results because w_c is close to zero at these distances from the cone tip. Second, the computation of w_c by Equation 3 is restricted to points that fall within the depth limits of the CPT sounding (i.e., the filter window is truncated at the data boundaries). This restriction ensures that the total area under the filter remains equal to unity near the upper and lower limits of the CPT sounding.

The behavior of the filter model is illustrated in Figure 5 showing q' and q^m versus depth for three idealized soil profiles that each have four layers of a stronger soil interbedded in a weaker soil. The stronger soil has $q' = 100$ in all cases, whereas the weaker soil has $q' = 1, 10, \text{ and } 50$ in Figures 5a, 5b, and 5c, respectively. The four stronger layers have thicknesses of 5, 10, 20, and 60 cone diameters in all cases. The digital data for these idealized profiles was generated with a uniform 20 mm sampling interval. The peak q^m that is computed

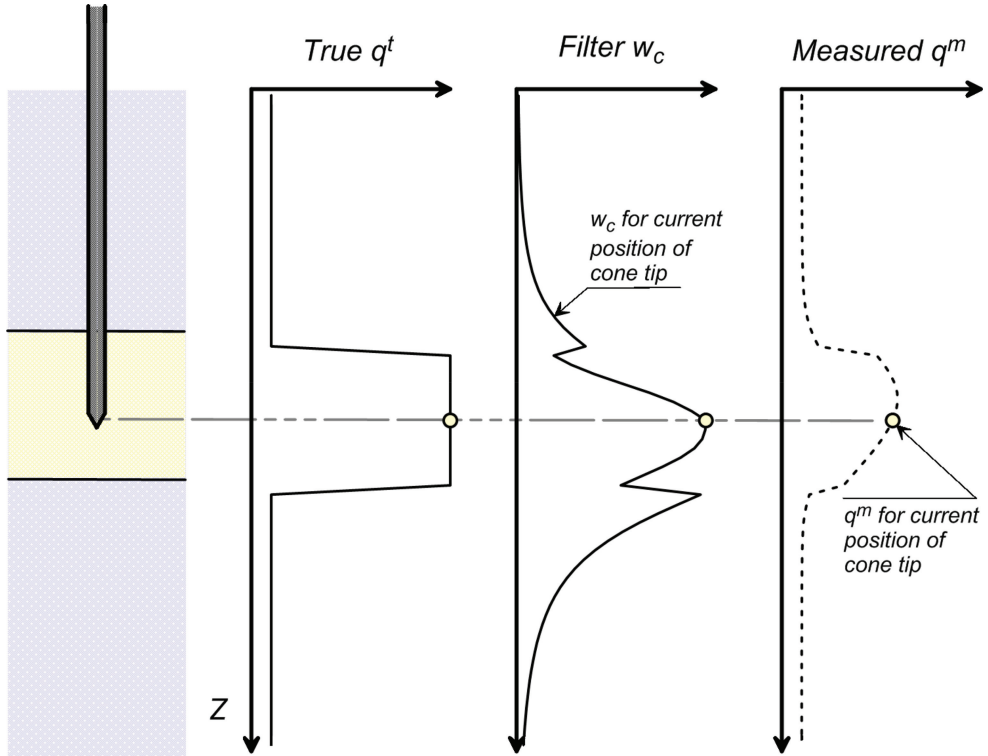


Figure 4. Illustration of the convolution of q^t with the cone penetration filter to obtain q^m at a given point in a layered profile.

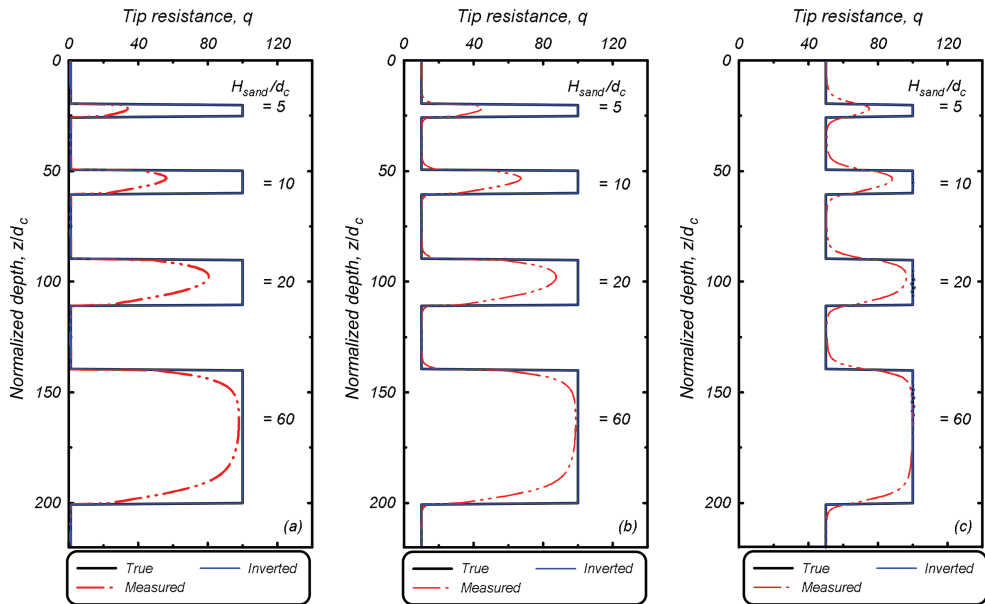


Figure 5. Values of q^t , q^m and q^{inv} for idealized profiles with interlayers of a strong soil with $q^t = 100$ embedded in a weaker soil with: (a) $q^t = 1$, (b) $q^t = 10$, and (c) $q^t = 50$. Note that q^{inv} almost perfectly overlays q^t .

to develop in the stronger layers decreases with decreasing layer thickness and decreasing strength in the surrounding soils.

Thin layer correction factors were subsequently derived using the above type of analysis for a uniform strong layer embedded in a uniform weaker deposit (e.g., Figure 1), with the results summarized in Figure 6. The derived values of K_H increase as q_{strong}^t/q_{weak}^t increases, but the rate of increase in K_H diminishes as q_{strong}^t/q_{weak}^t becomes larger. The K_H values approach unity for layers thicknesses greater than about 40 cone diameters, and are between 1.5 and 1.9 for layers about 10 cone diameters thick with q_{strong}^t/q_{weak}^t of 10–100. These K_H values are

reasonably consistent with those of prior experimental and theoretical studies. The values of K_H increase rapidly as the thickness of the strong layer becomes less than about 5–10 cone diameters.

Sensing and development distances were similarly derived for an idealized two-layer system having q_{upper}^t/q_{lower}^t ratios ranging from 0.02 to 50. The sensing distance for the cone when it is in the upper layer (Δz_{sens}) and the development distance for the cone when it has entered the lower layer (Δz_{dev}), were determined as the distances from the interface where the difference between q^m and q^t was 5, 10, or 20%. The resulting values for $\Delta z_{sens}/d_c$ and $\Delta z_{dev}/d_c$ are plotted versus q_{upper}^t/q_{lower}^t in Figures 7a

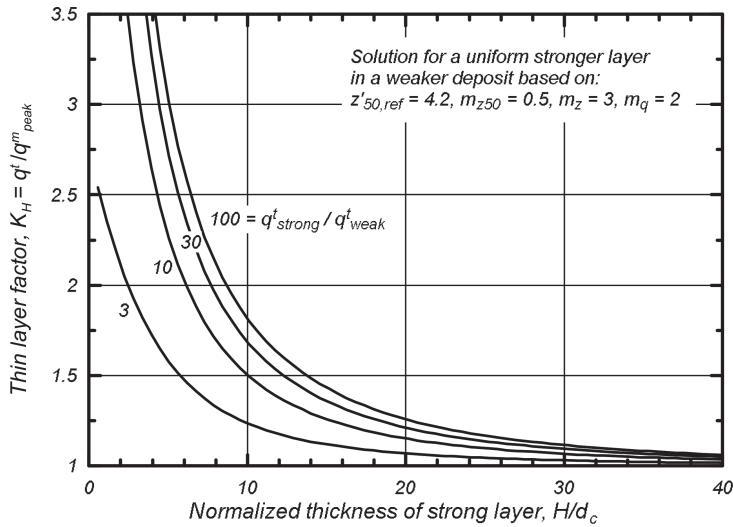


Figure 6. Thin layer correction factors computed for a uniform stronger layer of thickness H in a uniform weaker deposit.

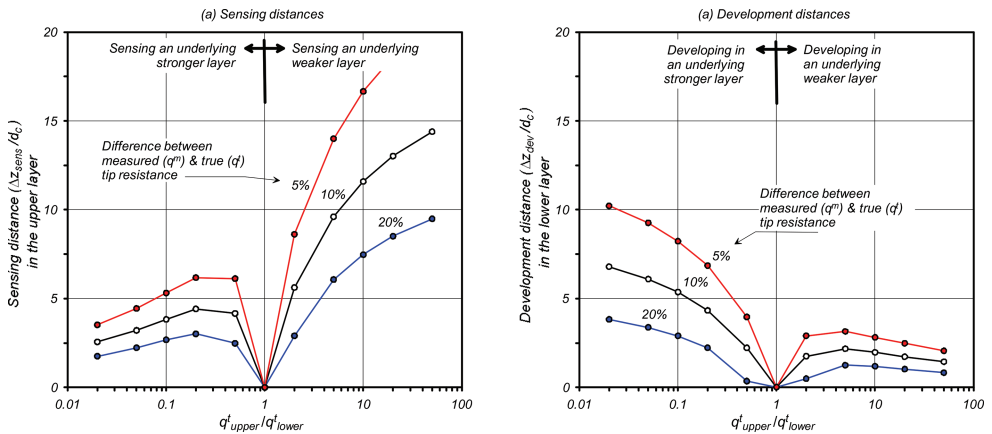


Figure 7. Sensing and development distances for a two layer system: (a) sensing distances, and (b) development distances.

and 7b, respectively. The $\Delta z_{\text{sens}}/d_c$ ranges from 2 to 6 when the cone is sensing an underlying stronger layer (left side of Figure 7a) and can be as large as 10–20 when the cone is sensing an underlying weaker layer (right side of Figure 7a). The $\Delta z_{\text{dev}}/d_c$ ranges from 2 to 10 when the cone is developing in an underlying stronger layer (left side of Figure 7b) and can be as small as 1 to 3 when the cone is developing in an underlying weaker layer (right side of Figure 7b).

The functional forms of the filter and the calibration of the filter parameters, as presented in this section, were iteratively developed to be consistent with the available experimental and theoretical data on thin layer and transition zone behaviors discussed in the previous section. The filter parameters can be adjusted to increase or decrease the thin layer effects or the sensing and development distances; for example, increasing Z_{sofref} will cause the sensing/development distances to increase and the thin layer factors to increase for a given sand layer thickness. The parameter values adopted herein are considered reasonable values for general application, pending further experiences and validation studies.

5 SOLUTION PROCEDURE

5.1 Inversion for tip resistance

Inversion of q^m to obtain an estimate of q^t requires an iterative solution procedure because the filter is nonlinearly dependent on the unknown q^t . A method of successive substitutions as outline below was found to work well. The basic equations are first rearranged to obtain the difference between q^t and q^m as,

$$dq = q^t - q^m \quad (9)$$

where q^m is equal to the convolution of q^t with the filter, leading to

$$dq = q^t - q^t * w_c \quad (10)$$

The value of q^t can then be determined as,

$$q^t = q^m + dq \quad (11)$$

$$q^t = q^m + (q^t - q^t * w_c) \quad (12)$$

The above equation can now be solved by successive iterations as,

$$q_{n+1}^{\text{inv}} = q^m + (q_n^{\text{inv}} - q_n^{\text{inv}} * w_c) \quad (13)$$

where q_n^{inv} is the result of the n^{th} iteration. The iteration process is initiated with the first estimate

of q^{inv} set equal to q^m . Iterations continue until the following error criterion is satisfied,

$$\text{err} = \frac{\sum |(q_{n+1}^{\text{inv}} - q_n^{\text{inv}})_i|}{\sum |(q^m)_i|} < 10^{-6} \quad (14)$$

This solution procedure, without any adjustments, is not well constrained at spatial frequencies that are higher than justifiable based on the data sampling interval or the physical size of the cone. These higher-than-justifiable spatial frequency components can also impede convergence of the solution, as shown later. Two additional steps were therefore added to the solution procedure to remove these higher spatial frequencies and improve convergence; these additional steps are introduced in sequence below, after first illustrating performance of the solution procedure without either additional step.

Performance of the above solution procedure (without the additional steps) is illustrated in Figure 5, which shows an idealized q^t profile along with a q^m computed by convolving q^t with the baseline filter model. Also shown in these plots are the q^{inv} computed iteratively from q^m with the same or “true” filter. For the cases in Figures 5a and 5b, the solution procedure converged and the differences between q^{inv} and q^t are negligible. These cases illustrate how the solution procedure is essentially perfect if the filter is known perfectly and the solution converges. For the case in Figure 5c, the solution procedure did not converge, but rather stabilized at a solution where q^{inv} included a small amount of low-level, high spatial frequency (short wavelength) noise in the stronger layers (barely visible as ripples in the q^{inv}). The wavelength of this noise is similar to the cone tip length, which is when the solution process can become less stable.

The potential effects of “noise” or the potential challenges with inverting information from very thin interlayers using the above solution procedure is further illustrated in Figure 8(a). This figure shows a profile of uniform soil with $q^m = 10$ except for thin intervals that are 1.1, 1.7, 2.2, and 3.4 cone diameters thick and have $q^m = 12$. The digital data were generated with a uniform 20 mm sampling interval, such that these depth intervals correspond to 2, 3, 4, and 6 data points with $q^m = 12$. Inversion of this q^m profile did not converge (i.e., meet the error criteria), but did stabilize at the solution shown in Figure 8a with peak q^{inv} values in the range of 30–40. These high q^{inv} values are sensitive to details of the filter model and are not reliable.

The solution procedure therefore requires an additional smoothing step that removes some of the highest spatial frequencies (shortest wavelengths) during the inversion process. After each

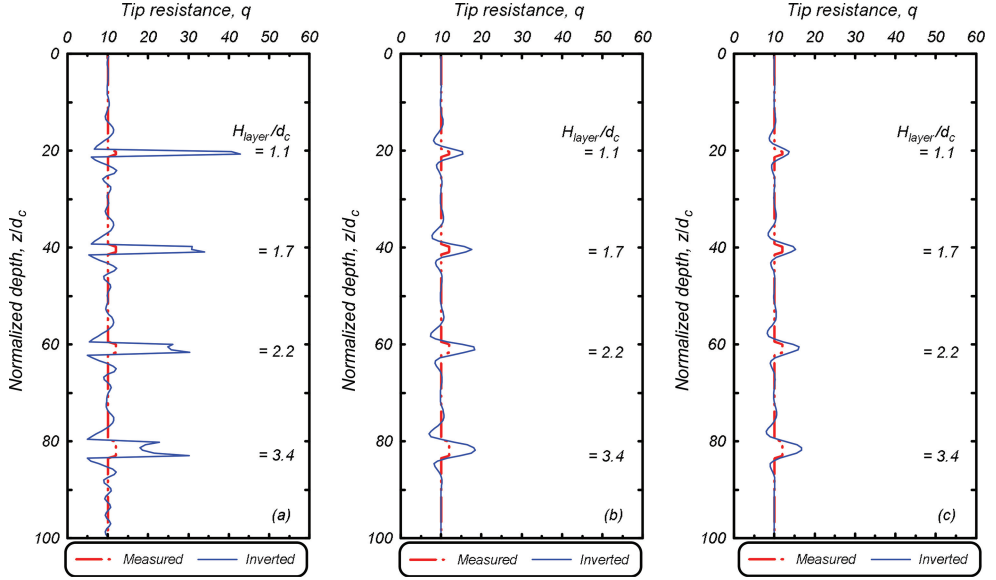


Figure 8. Inversion for a profile that has thin interlayers with $q^m = 12$ embedded in a uniform deposit having $q^m = 10$: (a) results using the first solution procedure, (b) results for the solution procedure with smoothing over the cone tip length, and (c) results for the solution procedure with smoothing followed by low-pass spatial filtering.

iteration, q^{inv} is smoothed (or low-pass spatial filtered) by taking a moving average over a window of a specified number of data points. The smoothing window is defined as the larger of either three points or the ceiling (rounding up) of the cone tip length (i.e., $0.866 d_c$) divided by the data point depth spacing (i.e., Δz). The first criterion governs for a standard 10 cm^2 cone and uniform 20 mm data sampling interval, whereas the second criterion governs if the data sampling interval is much smaller (e.g., 5 mm). In this regard, the solution procedures were tested for data sampling intervals of $1\text{--}50 \text{ mm}$ to ensure they continued to perform well for non-standard conditions. The inclusion of this smoothing step removes spatial frequencies that cannot be reliably inverted, greatly improves the convergence rate, and eliminated any cases of non-convergence. For example, application of the revised solution procedure to the profile shown in Figure 8 produced the smoother and more reasonable results shown in Figure 8b. In addition, the error term is plotted versus iteration number in Figure 9 for the solution procedures used for Figures 8a and 8b, illustrating how the inclusion of smoothing greatly improved the numerical performance of the solution procedure.

A second low-pass spatial filtering step was added to the solution procedure, although its effects are small for most situations. For this last step, the converged q^{inv} from the inversion with smoothing is convolved with another low-pass filter,

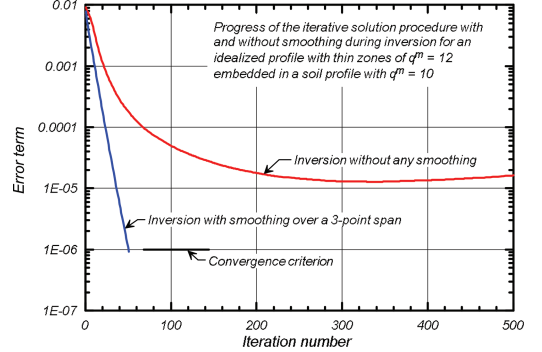


Figure 9. Progress of the iterative soil procedure with and without smoothing during inversion.

$$q^{\text{inv}} = q^{\text{inv}} * w_{c2} \quad (15)$$

where w_{c2} is the same filter model as w_c except that $z_{50\text{ref}}$ is reduced to the length of the cone tip (i.e., $0.866 d_c$). The application of this additional step in the inverse filtering of the profile shown in Figure 8 produced the slightly smoother result shown in Figure 8c. The results in Figure 8c illustrate that the overall solution procedure with smoothing during inversion followed by low-pass spatial filtering appears well-suited for handling high spatial frequency noise.

Performance of the overall solution procedure (inversion with smoothing followed by low-pass

spatial filtering) is illustrated in Figure 10 for the same idealized profiles examined previously (in Figure 5). The q^{inv} profiles still reasonably approximate the q^t profiles, though slightly rounded at the interfaces and slightly smaller than q^t for the inter-layers that are only 5 cone diameters thick.

Performance of the overall solution procedure can also be expressed in terms of the “net” thin-layer factor that it produces for idealized two-layer systems, as shown in Figure 11. These net factors are computed as the peak q^{inv} in a thin layer divided by the peak q^m for that same layer, and thus are

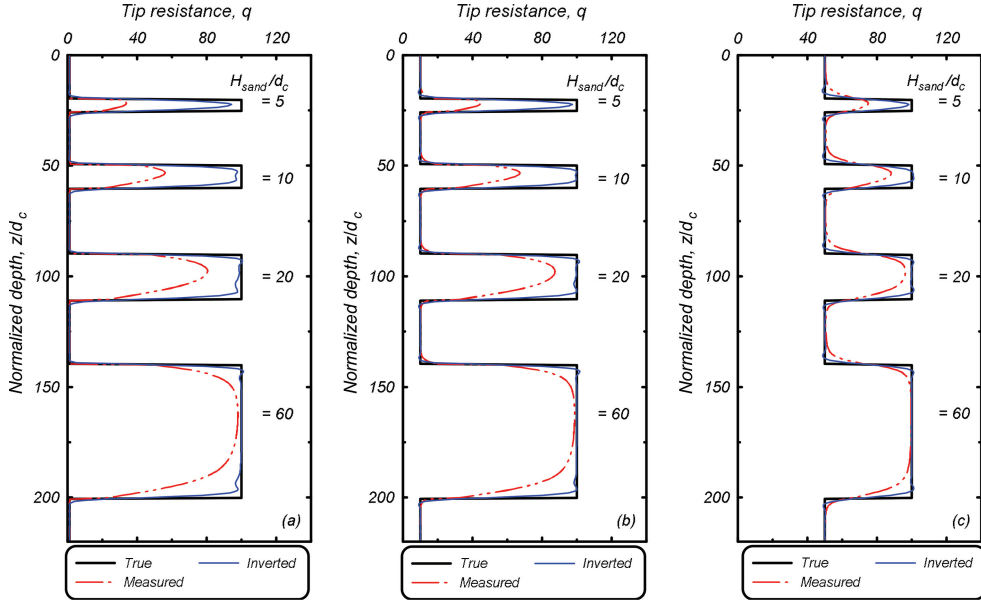


Figure 10. Values of q^t , q^m and q^{inv} for three idealized profiles using the solution procedure with smoothing followed by low-pass spatial filtering. Stronger layers have $q^t = 100$ and the weaker layers have (a) $q^t = 1$, (b) $q^t = 10$, and (c) $q^t = 50$.

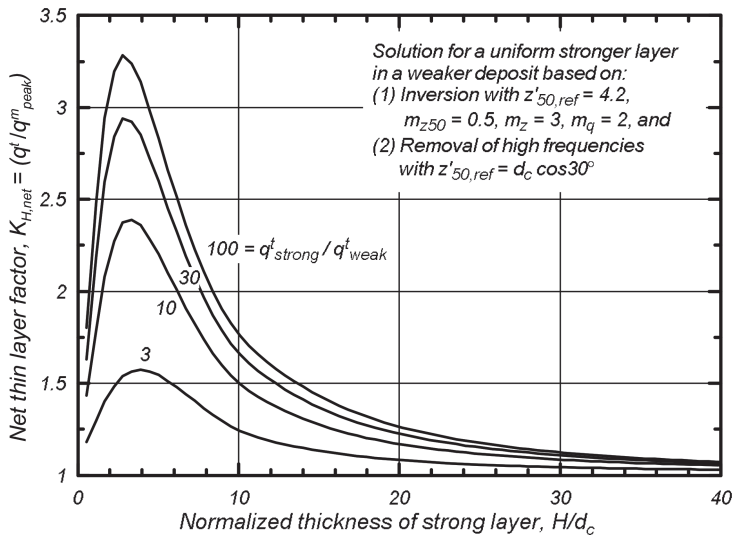


Figure 11. Net thin layer correction factors computed using inversion with low-pass spatial filtering.

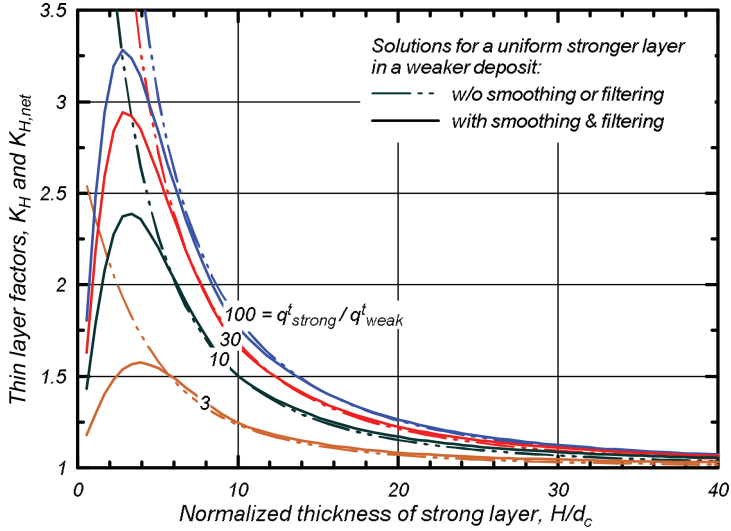


Figure 12. Comparison of the thin layer correction factors from the solutions with and without the smoothing and low-pass spatial filtering steps.

illustrative of how much amplification the inversion process may apply to the q^m in sand layers of various thicknesses. The $K_{H,net}$ curves for a range of q^t_{strong}/q^t_{weak} ratios all reach their peak values at strong-layer thicknesses of 3–4 cone diameters, and decrease toward unity with decreasing layer thickness. The fact $K_{H,net}$ tends to unity as the strong-layer thickness tends to zero reflects the fact that cone penetration measurements cannot provide meaningful information on soil properties when they vary strongly across interlayers that are less than about 2 or 3 cone diameters thick. The previously presented K_H values are overlain with the $K_{H,net}$ values in Figure 12, illustrating how the K_H values rapidly increase toward large values at these small layer thicknesses, which relates to why inversion without smoothing or low pass spatial filtering performed poorly. The solution procedure with smoothing during inversion followed by low-pass spatial filtering produces equivalent $K_{H,net}$ values that are reasonable for strong-layer thicknesses that are greater than about 3–4 cone diameters and appropriately conservative for thinner layers where inversion is not reliable.

5.2 Inversion for sleeve friction

The inversion of sleeve friction (f_s) profiles could conceptually follow a similar process as used for tip resistance. The filter model for f_s could have a different form and distribution. For example, examination of field data illustrates that f_s is more sensitive to thin layers than q_t , which would imply

a smaller zone of influence or greater weighting of data near the sleeve. Unfortunately, there are currently limited data available to guide development of a separate filter model for f_s .

The strategy adopted herein was to develop f_s^{inv} values from the q^{inv} values. This procedure assumes that the pairs of normalized tip resistance (Q) and normalized sleeve friction ratio (F) for the inverted and measured data lie along a radial line originating from the origin of the Soil Behavior Type Index (I_c). The values of Q and F are computed as,

$$Q = \left(\frac{q - \sigma_{vc}}{P_a} \right) \left(\frac{P_a}{\sigma'_{vc}} \right)^n \quad (16)$$

$$F = \left(\frac{f_s}{q - \sigma_{vc}} \right) 100\% \quad (17)$$

where σ_{vc} is the total vertical stress, σ'_{vc} is the effective vertical stress, and P_a is atmospheric pressure. The stress exponent n is computed following the relationship recommended by Robertson (2009),

$$n = (0.38I_c + 0.05\sigma'_{vc} - 0.15) \leq 1 \quad (18)$$

and the value of I_c is computed using the form recommended by Robertson and Wride (1997),

$$I_c = \left[(3.47 - \log(Q))^2 + (1.22 + \log(F))^2 \right]^{0.5} \quad (19)$$

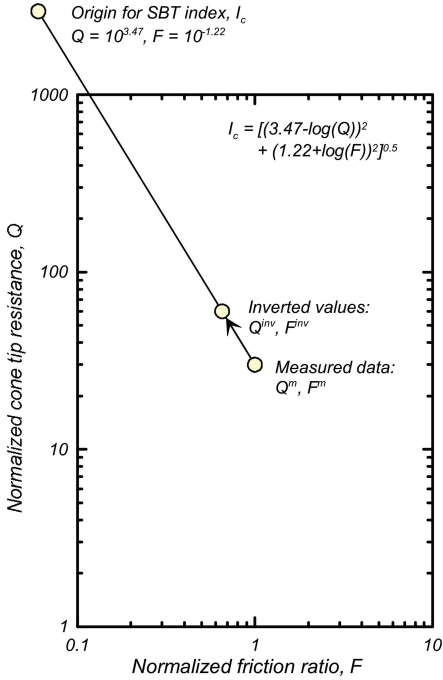


Figure 13. Procedure used to compute F^{inv} given Q^m and F^m for the field measurements and the value of Q^{inv} obtained from the inversion procedure.

The I_c value can be visualized as the radial distance between any Q-F pair and an origin point located at $Q = 2,951$ and $F = 0.0603$, as shown in Figure 13. The measured q^m and f_s^m values are used to compute Q^m and F^m values, and the inverted q^{inv} is used to compute a Q^{inv} value. The value of F^{inv} is then computed based on the assumption that the inverted point moved radially with respect to the I_c origin,

$$F^{inv} = 10^{\left\{ \frac{(3.47 - \log(Q^{inv}))}{(3.47 - \log(Q^m))} \left((1.22 + \log(F^m)) - 1.22 \right) \right\}} \quad (20)$$

The above procedure is schematically illustrated for a single data point in Figure 13. The value of f_s^{inv} is then computed from F^{inv} using the definition of F .

6 INTERFACE DETECTION AND CORRECTION

The detection of sharp interfaces and correction of the data at those interfaces is a separate step because the inversion process does not reproduce the high-spatial frequencies associated with a step

in the q^t profile (i.e., the smoothing during inversion followed by low-pass spatial filtering removes those spatial frequencies because they cannot be inverted reliably). Identifying sharp transitions is complicated by the fact that some interfaces may be sharp and others may be graded (e.g., upward fining sequences), and thus the criteria and process will involve some subjectivity and should be subject to confirmation by borehole sampling data or knowledge of local geology.

A sharp transition (or interface) is considered likely to exist if the rate of change in the logarithm of q^{inv} with respect to normalized depth is larger than a specified criterion. The rate of change across each discrete data sampling interval is computed as,

$$m_i = \frac{\ln(q_{i+1}^{inv}) - \ln(q_i^{inv})}{z'_{i+1} - z'_i} \quad (21)$$

Note that the index for m corresponds to the intervals between measurement points; i.e., if there are N points in the q^{inv} vector, there are $N-1$ points in the m vector. The value of m that would be consistent with the existence of a sharp interface can be estimated using experimental and theoretical estimates of the sensing and development distances. For example, if q changes by a factor of more than 2 over a distance of about 6 cone diameters (214 mm for a standard 10 cm² cone), then m will exceed 0.12 on average. On the other hand, if q smoothly changes by a factor of less than 10 over a graded interval that is about 1 m thick (or about 28 standard cone diameters), then m may not exceed 0.08 on average. Thus, a sharp interface may be expected to exist if m exceeds a specified threshold, m_t . A reasonable value for m_t , as adopted herein, may be on the order of 0.1, subject to refinement based on site-specific sampling and geologic information.

The transition zone over which q^{inv} at a sharp interface is still blurred will also have smoothly varying m values. The m values both above and below the point where the maximum m is obtained will be smaller than the maximum m for that transition zone. For the present study, the transition zone is assumed to include any contiguous measurement points where m is greater than $m_t/5$. If the zone identified by the above criteria is less than 3 cone diameters thick, then is it is not considered a transition zone. If the zone identified by the above criteria is greater than 12 cone diameters thick where q^{inv} is increasing, then the interval is truncated to 12 cone diameters thick (centered on the original zone). If the zone identified by the above criteria is greater than 18 cone diameters thick where q^{inv} is decreasing, then the interval is truncated to

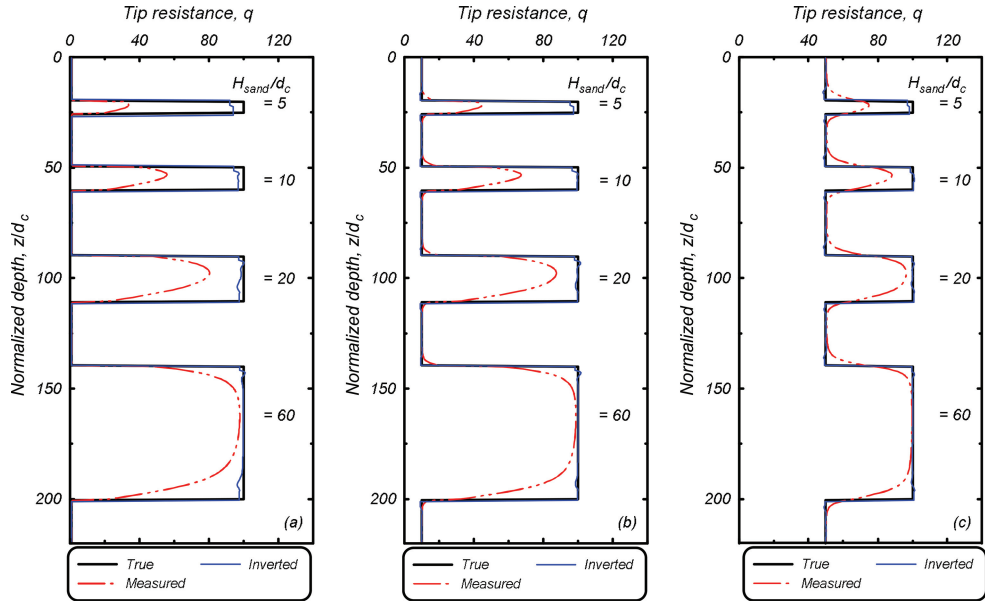


Figure 14. Values of q^t , q^m and q^{inv} for three idealized profiles using inversion with smoothing followed by low-pass spatial filtering and interface detection and correction. Stronger layers have $q^t = 100$ and the weaker layers have (a) $q^t = 1$, (b) $q^t = 10$, and (c) $q^t = 50$.

18 cone diameters thick (centered on the original zone). Once the transition zone has been defined, the q^{inv} and f_s^{inv} values at the top of the transition zone are assigned to all points in the upper 40% of the transition zone for penetration advancing into a stronger layer or the upper 60% of the transition zone for penetration advancing into a weaker layer. The q^{inv} and f_s^{inv} values at the bottom of the transition zone are assigned to all remaining points in the lower part of the transition zone.

Application of the interface detection and correction algorithm is illustrated in Figure 14 for the same idealized profiles presented in Figures 5 and 10. The interface detection and correction algorithm does not perfectly remove the transition zone, since it does not capture the slow rates of change in q at the start and end of each transition zone for this idealized profile. A greater portion of the interface could be removed by reducing m_c , but that can result in falsely identifying transition zones or computing overly thick transition zones when processing real CPT soundings.

7 INVERSION EXAMPLES FOR FIELD DATA

7.1 Applications using the baseline model

Application of the proposed inverse filtering procedure is illustrated in Figures 15–18 for cone soundings from four different sites. The inversion,

low-pass spatial filtering, and interface detection steps are applied using the same baseline parameters specified in the previous sections. The first example (Figure 15) is CPT UC-4 along Sandholdt Road in Moss Landing, CA, USA where liquefaction-induced ground deformations were observed after the 1989 $M_w = 6.9$ Loma Prieta earthquake (Boulanger et al. 1997). The second example (Figure 16) is CPT 1–24 along Çark Canal in Adapazari, Turkey where no surficial evidence of liquefaction was observed after the 1999 $M_w = 7.5$ Kocaeli earthquake (Youd et al. 2009). The third example (Figure 17) is CPT 45185 at St. Theresa's school in Riccarton, Christchurch, New Zealand where no surficial evidence of liquefaction was observed during the 2010–2011 Canterbury Earthquake Sequence (Cox et al. 2017). The fourth example (Figure 18) is a CPT at Hinode Minami Elementary School, Urayasu, Japan where no evidence of liquefaction was observed following the 2011 $M_w = 9.0$ Tohoku earthquake (Cox et al. 2013). The data sampling intervals for these four CPT soundings were 50, 20, 10, and 25 mm, respectively. The latter three sites are of interest because some degree of liquefaction would have been expected based on common engineering liquefaction evaluation procedures, as reported in the various references. The details of liquefaction evaluations for each site are beyond the scope of the present paper, except to note that thin-layer and transition effects are considered to be one

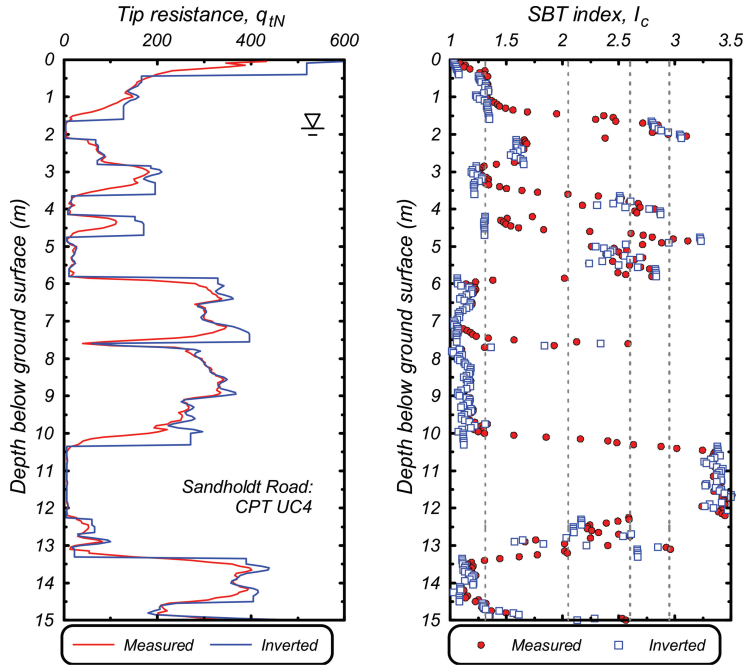


Figure 15. Measured and inverted q_{tN} and I_c profiles for CPT UC-4 at Sandholdt Road.

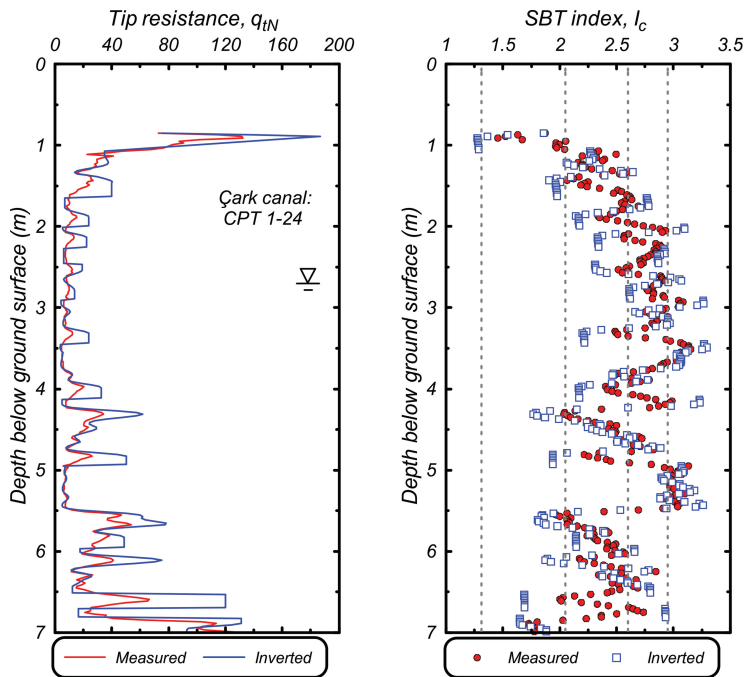


Figure 16. Measured and inverted q_{tN} and I_c profiles for CPT 1-24 at Çark Canal.

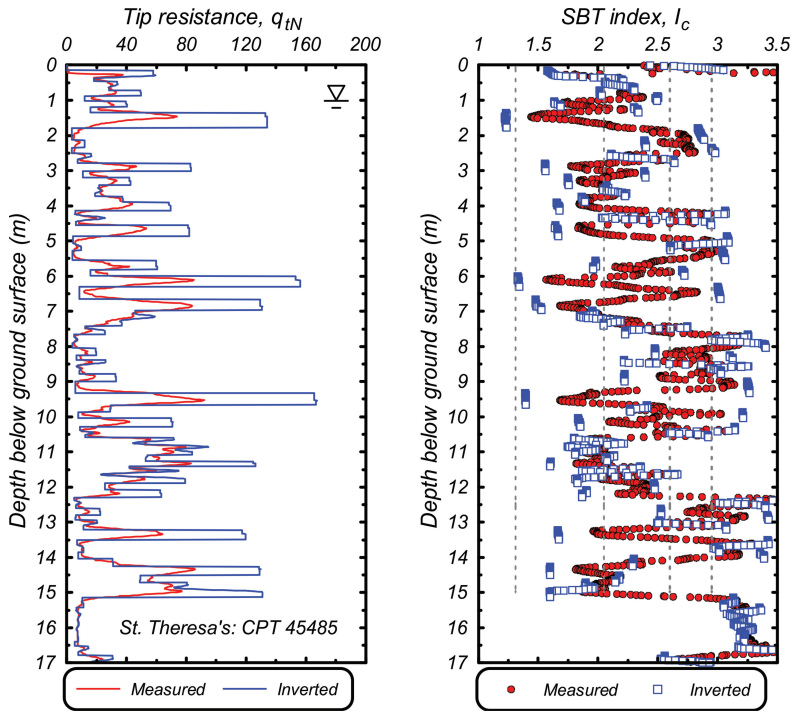


Figure 17. Measured and inverted q_{tN} and I_c profiles for CPT-45185 at St. Theresa's School.

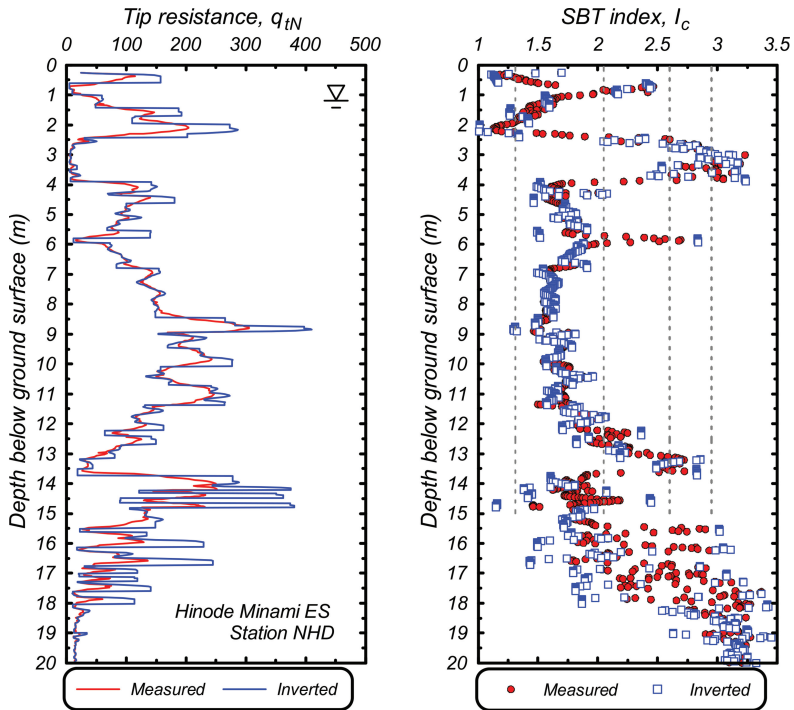


Figure 18. Measured and inverted q_{tN} and I_c profiles for Station NHD at Hinode Minami Elementary School.

of several factors that can contribute to the over-prediction of liquefaction effects (e.g., Boulanger et al. 2016).

Examination of these four examples illustrates that the proposed CPT inversion procedure is performing as expected. The inversion process has negligible effects on q or I_c in intervals where the soil type or penetration resistance is relatively uniform. The inversion procedure has the greatest

effect where well-defined thin-layers of stronger material are detected. The inversion procedure increases q^{inv} (relative to q^m) by factors up to 2–3 even for the thinnest strong interlayers at the highly interbedded sites, which reflects the upper limits that the present inversion parameters will produce (e.g., as illustrated by the net thin layer factors in Figure 11) and that can be justified given conventional cone diameters. The inversion procedure was

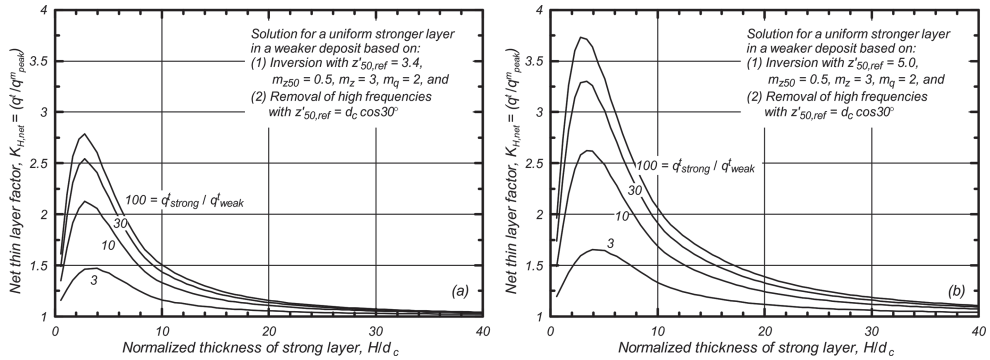


Figure 19. Net thin layer correction factors using the baseline set of filter parameters except for: (a) $z'_{50,ref} = 3.4$, and (b) $z'_{50,ref} = 5.0$

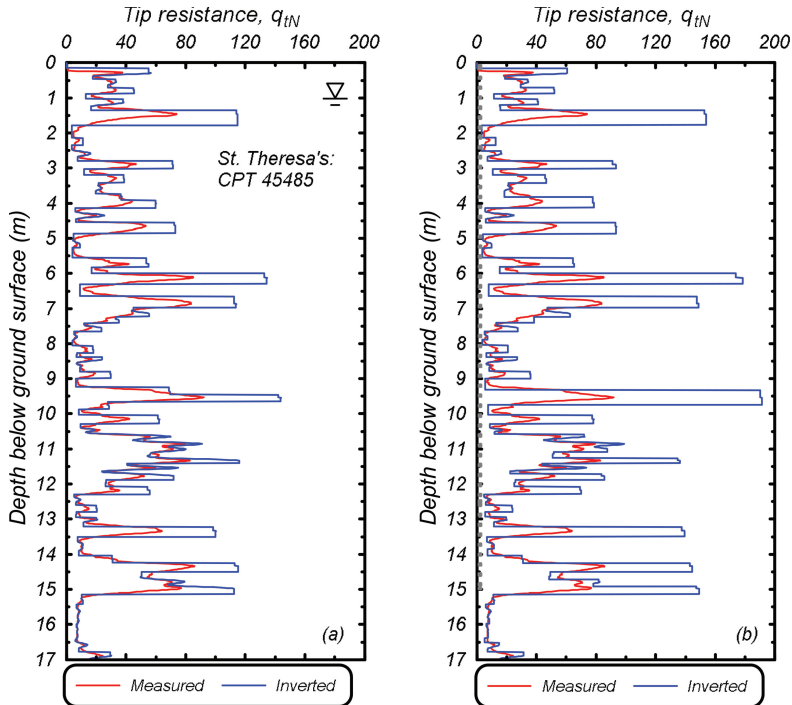


Figure 20. Measured and inverted q_{tN} profiles for CPT-45185 at St. Theresa's School using the baseline set of filter parameters except for: (a) $z'_{50,ref} = 3.4$, and (b) $z'_{50,ref} = 5.0$.

effective in removing transition zones at clearly identifiable contacts, while the detection criteria left other zones of slowly increasing penetration resistance unmodified.

7.2 Example using alternative filter parameters

The sensitivity of the inverse filtering procedure to alternative sets of filter parameters was also evaluated, recognizing that there is uncertainty in the filter model and individual parameters. The effect of individual parameter variations were examined in terms of how they affected the solutions for idealized problems (e.g., Figure 14), sensing and development distances for idealized two layer profiles (e.g., Figure 7), net thin layer correction factors (e.g., Figure 11), and results for field CPT soundings. Alternative sets of parameters that are consistent with the body of available experimental and theoretical data can be developed, including sets that provide more or less aggressive corrections to measured data.

For example, consider the effect of setting $z'_{50,ref}$ equal to 3.4 or 5.0 ($\pm 19\%$ from the baseline value of 4.2), while keeping all other parameters equal to the baseline values. The corresponding $K_{H,net}$ values, as shown in Figures 19a and 19b, are smaller for $z'_{50,ref} = 3.4$ and larger for $z'_{50,ref} = 5.0$, with the differences being larger for smaller layer thicknesses. For a strong layer thickness of 3–5 cone diameters, using $z'_{50,ref} = 3.4$ reduced the $K_{H,net}$ values by 8–18% (relative to those for the baseline set of filter parameters) whereas using $z'_{50,ref} = 5.0$ increased the $K_{H,net}$ values by 6–18%.

The effects of using the above $z'_{50,ref}$ values on the inverse filtering of a field CPT sounding are illustrated in Figures 20a and 20b for CPT 45185 at St. Theresa's school in Riccarton. The use of $z'_{50,ref} = 3.4$ (Figure 20a) resulted in smaller q_t values in the numerous thin sand interlayers relative to those for the baseline case (Figure 17), whereas use of $z'_{50,ref} = 5.0$ (Figure 20b) resulted in larger q_t values. The differences in the inversion results for these two cases are consistent with the differences in the corresponding net thin layer correction factors.

8 CONCLUDING REMARKS

An inverse filtering procedure for developing estimates of the “true” cone penetration tip resistance and sleeve friction values from measured cone penetration test data was presented. The inverse filtering procedure has three primary components: (1) a model for how the cone penetrometer acts as a low-pass spatial filter in sampling the true distribution of soil resistance versus depth, (2) a solution procedure to iteratively determine an estimate of

the true cone penetration resistance profile from the measured profile given the cone penetration filter model, and (3) a procedure to identify sharp transition interfaces and correct the data at those interfaces. The inverse filtering procedure was shown to produce equivalent thin layer factors and sensing/development distances that are consistent with the results of prior experimental and theoretical studies. Example applications of the inverse filtering procedure to four CPT soundings illustrated that the model performs well for a range of soil profile characteristics. The inverse filtering procedure was shown to provide an objective, repeatable, and automatable means for correcting cone penetration test data for thin-layer and transition zone effects.

Further experience with application of the inverse filtering procedure can be expected to lead to improvements in components of the procedure or improved guidance for its use in practice. Issues worth further examination include how f_s and q_c may filter differently, how the filter model might depend on other specific properties (stiffness, strength, drainage conditions) or stratigraphic sequences, and how the inversion process or parameters might be adjusted based on site-specific borehole and geologic information. The present model was developed with a focus on liquefaction problems, whereas applications to other problems may identify different aspects that warrant improvement. Regardless of advances, there will be practical limits to how well inverse filtering procedures, or any other technique, can correct cone penetration test data given the nature of the cone penetration process, the infinite possible variations in geologic conditions, the presence of noise in measurements, and other complex processes that influence the measurements (e.g., partial drainage, physical dragging of soil along with the cone). In this regard, the proposed inverse filtering procedure is intended to improve or enhance the field measurements, while recognizing that any inversion process will be neither unique nor perfect.

ACKNOWLEDGMENTS

The authors appreciate the financial support of the National Science Foundation (award CMMI-1635398) and California Department of Water Resources (contract 4600009751) for different aspects of the work presented herein. Any opinions, findings, conclusions, or recommendations expressed herein are those of the authors and do not necessarily represent the views of these organizations. Dr. Mohammad Khosravi and Mr. Mathew Havey contributed to the literature review and evaluation of alternative procedures for evaluating thin-layer effects. Dr. Dan

Wilson provided valuable comments on numerical aspects of inverse filtering procedures. Professor Brady Cox provided valuable review comments that improved the clarity of the paper. The authors appreciate the above support and interactions.

REFERENCES

- Ahmadi, M. M. and Robertson, P. K. 2005. Thin-layer effects on the CPT q_c measurement. *Canadian Geotechnical Journal*, 42(5), 1302–1317.
- Boulanger, R. W., Mejia, L. H., and Idriss, I. M. 1997. Liquefaction at Moss Landing during Loma Prieta Earthquake. *Journal of Geotechnical and Geoenvironmental Engineering*, ASCE, 123(5), 453–467.
- Boulanger, R. W., Moug, D. M., Munter, S. K., Price, A. B., and DeJong, J. T. 2016. Evaluating liquefaction and lateral spreading in interbedded sand, silt, and clay deposits using the cone penetrometer. *Geotechnical and Geophysical Site Characterisation 5*, B. M. Lehane, H. Acosta-Martinez, and R. Kelly, eds., Australian Geomechanics Society, Sydney, Australia, ISBN 978-0-9946261-2-7.
- Canou, J. 1989. Piezocone et liquefaction des sables. Rapport de synthese des travaux realises au CERMES, Re-search Report CERMES/ENPC, Paris, 176 p.
- Cox, B. R., Boulanger, R. W., Tokimatsu, K., Wood, C., Abe, A., Ashford, S., Donahue, J., Ishihara, K., Kayen, R., Katsumata, K., Kishida, T., Kokusho, T., Mason, B., Moss, R., Stewart, J., Tohyama, K., and Zekkos, D. 2013. Liquefaction at strong motion stations and in Urayasu City during the 2011 Tohoku-Oki earthquake. *Earthquake Spectra*, EERI, 29(S1), S55-S80.
- Cox, B. R., McLaughlin, K. A., van Ballegooy, S., Cubrinovski, M., Boulanger, R. W., and Wotherspoon, L. 2017. In-situ investigation of false-positive liquefaction sites in Christchurch, New Zealand: St. Teresa's School case history. Proc., Performance-based Design in Earthquake Geotechnical Engineering, PBD-III Vancouver, M. Taiebat et al., eds., ISSMGE Technical Committee TC203, paper 265.
- Cristobal, G., Schelkens, P., and Thienpont, H. 2011. Optical and digital image processing: Fundamentals and applications. Wiley-VCH Verlag GmbH & Co KGaA, Editors: G. Cristobal, P. Schelkens, and H. Thienpont, DOI: 10.1002/9783527635245.
- Foray, P. & Pautre, J-L. 1988. Piezocone et liquefaction des sables: synthese des essais sur sites en Nouvelle-Zelande et des essais en Chambre de Calibration a l'IMG, Research Report, IMG, Grenoble, 70 p.
- Hird, C. C., Johnson, P., and Sills, G. C. 2003. Performance of miniature piezocones in thinly layered soils. *Géotechnique*, 53(10), 885–900.
- Lunne, T., Robertson, P.K., and Powell, J.M. 1997. Cone penetration testing in geotechnical practice. Blackie Academic & Professional, London, UK.
- Mayne, P. 2007. Cone Penetration Testing—A synthesis of highway practice. NCHRP Synthesis 268, Transportation Research Board, Washington, D.C.
- Meyerhof, G. G. and Valsangkar, A. J. 1977. Bearing capacity of piles in layered soils. Proc. 9th Int. Conf. Soil Mech. Found. Engng, Japan 1, 645–650.
- Mlynarek, Z., Gogolik, S., and Poltorak, J. 2012. The effect of varied stiffness of soil layers on interpretation of CPTU penetration characteristics. *Archives of Civil and Mechanical Engineering*, 12, 253–264.
- Mo, P.-Q., Marshall, A. M., and Yu, H.-S. 2017. Interpretation of cone penetration test data in layered soils using cavity expansion analysis. *J. Geotechnical and Geoenvironmental Eng.*, 143(1), 10.1061/(ASCE)GT.1943-5606.0001577.
- Mo, P. Q., Marshall, A. M., and Yu, H. S. 2015. Centrifuge modelling of cone penetration tests in layered soils. *Géotechnique*, 65(6), 468–481.
- Munter, S. K., Boulanger, R. W., Krage, C. P., and DeJong, J. T. 2017. Evaluation of liquefaction-induced lateral spreading procedures for interbedded deposits: Cark Canal in the 1999 M7.5 Kocaeli earthquake. *Geotechnical Frontiers 2017, Seismic Performance and Liquefaction*, Geotechnical Special Publication No. 281, T. L. Brandon and R. J. Valentine, eds., 254–266.
- Robertson, P. K. 2009. Interpretation of cone penetration tests—a unified approach. *Canadian Geotechnical Journal*, 46, 1337–1355.
- Robertson, P. K. and Fear, C. E. 1995. Liquefaction of sands and its evaluation. Proc., 1st Int. Conf. on Earthquake Geotechnical Engineering, Ishihara, K. (ed), A. A. Balkema.
- Robertson, P. and Wride, C., 1998. Evaluating cyclic liquefaction potential using the cone penetration test. *Canadian Geotechnical Journal*, 35(3), 442–459.
- Sayed, S. M., and Hamed, M. A. 1987. Expansion of cavities in layered elastic system. *International Journal of Numerical and Analytical Methods in Geomechanics*, 11(2), 203–213.
- Silva, M. F., and Bolton, M. D. 2004. Centrifuge penetration tests in saturated layered sands. Proc. ISC-2 on Geotechnical and Geophysical Site Characterization, Viana da Fonseca and Mayne (eds), 377–384.
- Tehrani, F. S., Arshad, M. I., Prezzi, M., and Salgado, R. 2018. Physical modeling of cone penetration in layered sand. *Journal of Geotechnical and Geoenvironmental Engineering*, 144(1), 04017101, DOI:10.1061/(ASCE)GT.1943-5606.0001809.
- Treadwell, D.D. 1976. The influence of gravity, prestress, compressibility, and layering on soil resistance to static penetration. Ph.D. thesis, University of California at Berkeley, Berkeley, Calif.
- Van den Berg, P., De Borst, R. & Huetink, H. 1996. An Eulerian finite element model for penetration in layered soil. *International Journal of Numerical and Analytical Methods in Geomechanics*, 20, 865–886.
- Vreugdenhil, R., Davis, R. and Berrill, J. 1994. Interpretation of cone penetration results in multilayered soils. *International Journal of Numerical and Analytical Methods in Geomechanics*, 18(9), 585–599.
- Walker, J. and Yu, H.-S. 2010. Analysis of the cone penetration test in clay. *Géotechnique*, 60(12), 939–948.
- Xu, X. T., and Lehane, B. M. 2008. Pile and penetrometer end bearing resistance in two-layered soil profiles. *Géotechnique*, 58(3), 187–197.
- Youd, T. L., Idriss, I. M., Andrus, R. D., Arango, I., Castro, G., Christian, J. T., Dobry, R., Finn, W. D. L., Harder, L. F., Hynes, M. E., Ishihara, K., Koester, J. P., Liao, S. S. C., Marcuson, W. F., Martin, G. R., Mitchell, J. K., Moriwaki, Y., Power, M. S., Robertson, P. K., Seed, R. B., and Stokoe, K. H. 2001. Liquefaction resistance of soils: summary report from the

- 1996 NCEER and 1998 NCEER/NSF workshops on evaluation of liquefaction resistance of soils, *J. Geotechnical and Geoenvironmental Eng.*, ASCE 127(10), 817–33.
- Youd, T. L., DeDen, D. W., Bray, J. D., Sancio, R., Cetin, K. O. and Gerber, T. M. 2009. Zero-displacement lateral spreads, 1999 Kocaeli, Turkey, earthquake. *Journal of Geotechnical and Geoenvironmental engineering*, 135(1), 46–61.
- Yue, Z.Q., and Yin, J.H. 1999. Layered elastic model for analysis of cone penetration testing. *International Journal for Numerical and Analytical Methods in Geomechanics*, 23, 829–843.